A distributed resistance analogy for solid oxide fuel cells

Beale, S.; Zhubrin, S. V.

Publisher's version / Version de l'éditeur:
https://doi.org/10.1080/10407790590907930
Numerical Heat Transfer, Part B: Fundamentals; an International Journal of Computation and Methodology, 47, 6, pp. 573-591, 2005

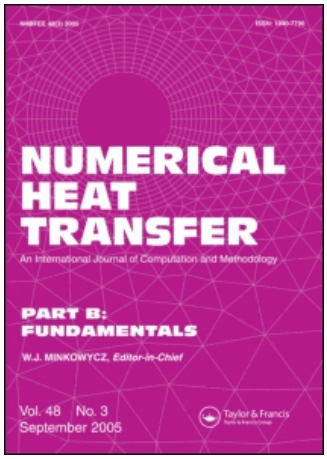

Numerical Heat Transfer, Part B: Fundamentals
An International Journal of Computation and Methodology
Publication details, including instructions for authors and subscription information:
http://www.informaworld.com/smpp/title~content=t713723316

A Distributed Resistance Analogy for Solid Oxide Fuel Cells

S. B. Beale [a]; S. V. Zhubrin [b]
[a] National Research Council, Montreal Road, Ottawa, Ontario, Canada
[b] Flowsolve Ltd., London, UK

Online Publication Date: 01 June 2005

To cite this Article: Beale, S. B. and Zhubrin, S. V. (2005) 'A Distributed Resistance Analogy for Solid Oxide Fuel Cells', Numerical Heat Transfer, Part B: Fundamentals, 47:6, 573 — 591

To link to this article: DOI: 10.1080/10407790590907930
URL: http://dx.doi.org/10.1080/10407790590907930

Numerical Heat Transfer, Part B, 47: 573–591, 2005

ISSN: 1040-7790 print/1521-0626 online
DOI: 10.1080/10407790590907930

A DISTRIBUTED RESISTANCE ANALOGY FOR SOLID OXIDE FUEL CELLS

S. B. Beale
National Research Council, Montreal Road, Ottawa, Ontario, Canada

S. V. Zhubrin
Flowsolve Ltd., London, UK

The method of distributed resistances is outlined for performance calculations in solid oxide fuel cells. The domain is discretized using a multiply shared space method. Both potentiostatic and galvanostatic conditions are considered. Mass transfer effects on the heat transfer coefficients and the Nernst potential are taken into consideration. Calculations, for one cell and for a 10-cell stack, are compared to those obtained using a detailed numerical method. Agreement is very good. It is concluded that the distributed resistance analogy may be used to predict transport phenomena in fuel cell stacks at a fraction of the computational cost required for conventional means.

INTRODUCTION

Distributed Resistance Analogy

The distributed resistance analogy was first introduced by Patankar and Spalding [1] in the context of heat exchanger design. The basic problem was one of scale: namely, that it was not possible to tessellate a heat exchanger containing numerous tubes, fine enough to capture the detailed flow around each individual tube on the shell side and at the same time be able to cover the entire domain, due to the large requirements for computer memory. Figure 1 is a schematic of one such heat exchanger. The solution proposed by the authors was to prescribe the resistance, F, and heat transfer coefficients, α, for the tubes in the bank, but still solve for the superficial flow around the baffles. The authors referred to this local volume averaging technique as a distributed resistance analogy (DRA). Values of the drag coefficient, f, and the Nusselt number, Nu, may be obtained either by

Received 28 July 2004; accepted 25 September 2004.
Dr. Wei Dong developed much of the DNM code, used to validate the DRA model, as a visiting postdoctoral fellow at the National Research Council of Canada. Prof. D. B. Spalding contributed some useful discussion about the DRA in the early stages of the project. Mr. Ron Jerome provided technical assistance. The support of the NRC Hydrogen and Fuel Cells Program is acknowledged with gratitude.
A preliminary version of this article was presented at CHT-04: An ICHMT International Symposium on Advances in Computational Heat Transfer, April 2004, G. de Vahl Davis and E. Leonardi (eds.), CD-ROM Proceedings, ISBN 1-5670-174-2, Begell House, New York, 2004.
Address correspondence to Steven B. Beale, National Research Council, Montreal Road, Ottawa, Ont. K1A 0R6, Canada. E-mail: steven.beale@nrc.ca

NOMENCLATURE

a	coefficient in finite-volume equations
A	area, m^2
B	driving force
b	blowing parameter
c	thermal capacitance, J/K
c_p	specific heat, J/kg K
C	source-term coefficient in finite-volume equations
D_h	hydraulic diameter, m
E	Nernst potential, V
f	friction coefficient
F	distributed resistance, $kg/m^2 s$;
$\mathcal{F}$	Faraday's constant, C/kmol
g	mass transfer conductance, kg/s
G	Gibbs free energy, J/kg, J/kmol
h	heat transfer coefficient per unit area, $W/m^2 K$
H	height, m; enthalpy, J/kg, J/kmol
i	current, A
j	source term in species equation, kg
k	thermal conductivity, W/m K
L	length, m
m	mass fraction, kg/kg; mass, kg
M	molecular weight, kg/kmol
n	electron number
Nu	Nusselt number
p	pressure, Pa
q	heat source term, J
r	resistance, Ω/m^2
R	gas constant, J/kmol K; resistance, Ω
Re	Reynolds number
S	source term, conduction shape factor
t	times, S
T	temperature, °C; temperature, K
u	interstitial velocity, m/s
U	overall heat transfer coefficient per unit area, $W/m^2 K$; superficial velocity, m/s
V	volume, m^3; cell potential, V; source-term value in finite-volume equations
x_i	mole fraction, kmol/kg
α	volumetric heat transfer coefficient, $W/m^3 K$
ϕ	general scalar
Γ	exchange coefficient, kg/m s
ε	volume fraction
η	overpotential; polarization, V
μ	viscosity, kg/m s
ρ	density, kg/m^3
τ	shear stress, N/m^2

Subscripts

a	air, anode
b	bulk
c	cathode
e	electrolyte
E	east neighbor
f	fuel
H	high neighbor
H_2	hydrogen
H_2O	water
i	interconnect, inlet
L	low neighbor
m	manifold
N	north neighbor
N_2	nitrogen
o	outlet
O_2	oxygen
P	in-cell
s	stack
S	south neighbor
t	transferred substance state
w	wall
W	west neighbor

Superscipts

0	reference state
*	zero mass transfer, at previous iteration
$\sim$	correction
$'$	per unit length
$''$	per unit area
$'''$	per unit volume
$\cdot$	per unit time

performing experiments, or from closed-form mathematical analysis, or by performing detailed numerical simulations for single tubes under periodic boundary conditions [2]. It is thus possible to perform calculations for the overall flow around the baffles, and the interfluid heat transfer, Figure 1*b*, providing information about the equipment performance, which could not reliably be obtained using traditional "presumed flow" analyses. More than a quarter-century later, and in spite of the vastly superior memory and speed available in computers today, the problem still

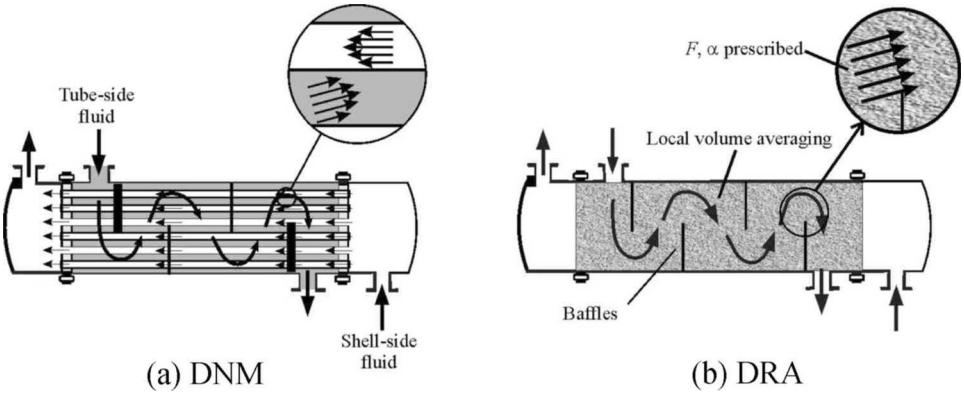

Figure 1. Shell-and-tube heat exchanger illustrating the distributed resistance analogy concept.

remains the same; and this methodology has been adopted as a design tool by some heat exchanger manufacturers.

The original problem considered by Patankar and Spalding [1] required only the shell-side flow field to be estimated, it being presumed that the tube-side flow field was sufficiently uniform so as not to require calculation. However, for many problems it is necessary that flow field calculations be performed simultaneously for both working fluids. A problem then arises with conventional computational fluid dynamics (CFD) codes that although algorithms exist for performing flow field calculations for two or more distinct "phases," generally speaking these only admit to a single value for pressure, p, at any given location (though in some problems, a second-phase pressure is defined which is a simple algebraic function of the regular pressure). In general, then, to solve flow field problems in which multiple yet distinct fluids are present, some special technique is required. To this end, the multiply shared space method (MUSES), described further below, was developed.

Solid Oxide Fuel Cell

The solid oxide fuel cell (SOFC) is a solid-state energy-conversion device which converts chemical energy to electricity and heat. The basic components of the SOFC are the anode, cathode, and electrolyte. The electrolyte is typically ytria-stabilized zirconia (YSZ), which allows O^{2-} ions produced at the cathode to pass to the anode, where they combine with negative electrons and fuel, presumed to be H_2, to form H_2O. SOFCs offer several potential advantages over other fuel cells, for example, a variety of fuels other than H_2, such as CH_4, may be used; the electrode–electrolyte assembly does not need to be humidified to function as a charge carrier, as in proton-exchange membrane fuel cells (PEMFCs); and the presence of trace elements, which can "poison" other fuel cell devices, are generally not a major problem in SOFC design. However, as a high-temperature device, operating in the range 800–1,000°C, a new set of problems arise, specifically, the mechanical integrity of the design due

to thermally induced stresses, as well as the temperature dependence of the electrochemical performance of the cell.

Fuel cells are typically stacked together to increase the overall voltage; Figure 2 shows one such configuration. Fuel and air are introduced through manifolds at the sides of the stack. The assembly is electrically in series but hydraulically in parallel. Interconnects, typically made out of stainless steel (or electrically conducting ceramic material) are used to effect the electrical connection, and also serve as a housing for the air and fuel channels. Uniformity of the flow field and pressure distributions is of paramount concern in stack design.

Electrochemical performance. It can be shown that the ideal or Nernst potential, $\boldsymbol{E}$, is given by

$$E = E^0 + \frac{RT}{2\mathcal{F}} \ln\left(\frac{x_{H_2} x_{O_2}^{0.5}}{x_{H_2O}}\right) + \frac{RT}{4\mathcal{F}} \ln p_a \tag{1}$$

where E^0 is a standard electrode potential, x is mole fraction, T is temperature, p_a is air pressure, and $\mathcal{F} = 96.485 \times 10^6 (\mathrm{C/Kmol})$ is Faraday's constant. Whenever an actual current flows in a fuel cell, the cell potential, V, is lower than the ideal value,

$$V = E - i'' r_e - \eta_a - \eta_c = E - i'' r \tag{2}$$

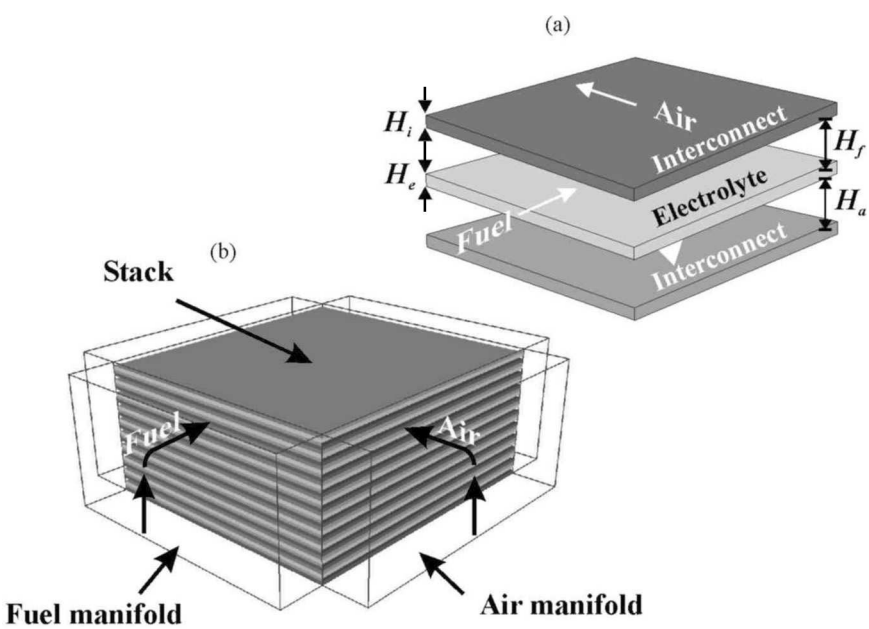

Figure 2. Schematic of fuel cell/stack geometry.

where i'' is the current density (A/m^2), η_a and η_c are anodic and cathodic "overpotentials" associated with activation for the electrode half-reactions (kinetic or charge-transfer rate-limiting factors), and r_e is the Ohmic resistance of the electrolyte. It is tacitly assumed that Ohmic losses in the metallic interconnects are negligibly small for the design under consideration. Generally speaking, the activation overpotentials are computed with a Butler-Volmer equation [3]. However, for convenience in developing the present model, all overpotentials were lumped as a single linearized internal resistance, r, in this work [4].

PROBLEM STATEMENT

The goal of this study was to develop a simplified CFD model for an industrial SOFC design. Previous DRA studies on SOFCs involved prediction of the flow fields only [5] and, more recently, the cell/stack temperature assuming a uniform heat source corresponding to an idealized case [6, 7]. This article is the first publication in which the entire electrochemical process, including nonuniform heat generation and mass transfer, is considered. A detailed numerical model (DNM) was used to validate the DRA, in the absence of high-quality experimental data.

The fuel cell is treated as a sandwich of four distinct materials: air, fuel, electrolyte (including the electrodes), and interconnect. For the process of developing the model theory, an idealized fuel cell prototype is considered in which it is presumed that all fluid and solid regions are simple rectangular-shaped zones. Figure 2*a* illustrates the cell geometry. Because the length and width are long compared to the height, H, the air and fuel passages may be treated as if they are planar ducts, simplifying the analysis considerably.

A single-cell and a stack of 10 cells were considered; Figure 2*b* shows the stack geometry. Air and fuel are admitted through risers or rectangular manifolds, pass across the cells in cross-flow, and are then exhausted through downcomers or outlet manifolds. Fuel cells may be operated in co-flow, counterflow, or cross-flow; however, only the latter is considered in this study. Material properties are given in Table 1.

Table 1 Properties of SOFC materials

	Fuel	Air	Electrolyte	Interconnect
Volume fraction	0.259	0.216	0.108	0.278
Density, ρ (kg/m^3)	0.255	0.399	3300	7700
Kinematic viscosity, ν(m^2/s)	1.53×10^{-4}	1.1286×10^{-4}	—	—
Specific heat, c_P (J/kg K)	1.6731×10^3	1.1283×10^3	598.1	450.0
Thermal conductivity, k (W/m K)	0.08	0.0672	2.0	25
Inlet interstitial velocity, u (m/s)	0.572	1.839	—	—
Inlet temperature, T (°C)	702	639	—	—
Inlet O_2 mass fraction, m_{O_2}	0	0.225	—	—
Inlet N_2 mass fraction, m_{N_2}	0.85	0.775	—	—
Inlet H_2 mass fraction, m_{H_2}	0.10	0	—	—
Inlet H_2O mass fraction, m_{H_2O}	0.05	0	—	—

Basic Theory

Let it be proposed that the governing equations are of the general form

$$\underset{\text{(i)}}{\frac{\partial(\rho_i\varepsilon_i\phi_i)}{\partial t}} + \underset{\text{(ii)}}{\nabla\cdot(\rho_i\varepsilon_i\mathbf{u}_i\phi_i)} = \underset{\text{(iii)}}{\varepsilon_i\sum_j \alpha_{ij}(\phi_j-\phi_i)} + \underset{\text{(iv)}}{\nabla\cdot(\varepsilon_i\Gamma_i\nabla\phi_i)} + \underset{\text{(v)}}{\varepsilon_i\dot{S}'''} \tag{3}$$

The terms in Eq. (3) are referred to as (i) transient, (ii) convection, (iii) interphase transfer, (iv) diffusion or within phase transfer, and (v) source. The reader will note that the convention of Jacob [8] is adopted, whereby a dot denotes a time derivative, and a dash a space derivative. Therefore, if q has units of joules, then $\dot{q}'''$ is in $\mathrm{W/m^3}$.

Continuity and Momentum

The continuity equation is straightforward, namely,

$$\frac{\partial(\rho_i\varepsilon_i)}{\partial t} + \nabla\cdot(\rho_i\varepsilon_i\mathbf{u}_i) = \varepsilon_i\dot{m}_i''' \tag{4}$$

Mass sources due to the electrochemical reactions are computed from Faraday's law,

$$\dot{m}_i'' = \pm\frac{M_i i''}{n_i\mathcal{F}} \tag{5}$$

where i'' is current density, M is molecular weight, $\mathcal{F}$ is Faraday's constant, and n is the electron number. In the DRA these are coded as volumetric sources, $\dot{m}_i''' = \dot{m}_i''/H_e$, where H_e is the height of the electrolyte.

The momentum equation is presumed to be of the form

$$\frac{\partial(\rho_i\varepsilon_i\mathbf{u}_i)}{\partial t} + \nabla\cdot(\rho_i\varepsilon_i\mathbf{u}_i\mathbf{u}_i) = -\varepsilon_i\nabla p_i + F_i\varepsilon_i^2(\mathbf{0}-\mathbf{u}_i) + \nabla\cdot(\varepsilon_i\mu_i\nabla\mathbf{u}_i) \tag{6}$$

The quantity F is referred to as a "distributed resistance" [1], and $\mathbf{u}$ is the local bulk interstitial velocity (the quantity $\mathbf{U} = \varepsilon\mathbf{u}$ is the so-called superficial velocity). For fully developed laminar duct flow, with negligible mass transfer,

$$f^* = \frac{\tau_w}{\frac{1}{2}\rho u^2} = \frac{a}{\mathrm{Re}} \tag{7}$$

where the asterisk denotes "at zero mass transfer." The Reynolds number, $\mathrm{Re} = D_h\rho u/\mu$, is based on a hydraulic diameter $D_h = 2H$, for planar geometry. It can readily be shown that

$$F^* = \frac{2a}{\varepsilon}\frac{\mu}{D_h^2} \tag{8}$$

with $a = 24$ for plane ducts; Shah and London [9] provide empirical relationships for rectangular and other ducts, obtained by numerical means. Within the stack, the viscous terms in the fluids are discarded. In the manifolds, however, these are nonzero, and it is the distributed resistance, F, that is set to zero.

Heat Transfer

The energy equation may be written in the form

$$\frac{\partial(\rho_i \varepsilon_i c_{pi} T_i)}{\partial t} + \nabla \cdot (\rho_i \varepsilon_i c_{pi} \mathbf{u}_i T_i) = \varepsilon_i \sum_j \alpha_{ij}(T_j - T_i) + \nabla \cdot (\varepsilon_i k_i \nabla T_i) + \varepsilon_i \dot{q}''' \quad (9)$$

Source terms. A heat source occurs due to Joule heating in the electrolyte. This is given by

$$\dot{q}''' = i'''(E - V) \quad (10)$$

where $i''' = i''/H_e$ is the current density per unit volume ($\mathrm{A/m^3}$). An additional heat source term is due to the fact that the molar Gibbs energy does not equate to the enthalpy of formation, and this fraction of the chemical energy must therefore be dissipated as heat at the anode, i.e., $\dot{q}'' = i''(\Delta G - \Delta H)/2\mathcal{F}$. For the purpose of model development, no distinction between volumetric and area source terms was made, and the two terms were combined as a single volumetric term.

Interphase heat transfer. Both terms (iii) and (iv) in Eq. (3) are present in Eq. (9). The volumetric heat transfer coefficients are computed as

$$\alpha V = UA \quad (11)$$

where A is the area for heat transfer, V is cell volume, and U is an overall heat transfer coefficient, obtained using harmonic averaging, for example,

$$\frac{1}{UA} = \frac{1}{hA} + \frac{H}{kAS} \quad (12)$$

where S is a conduction shape factor; with $S = 1$ for planar geometry, A is the surface area for heat transfer and H is the thickness of the solid region. Values of the heat transfer coefficient h^* were obtained from the appropriate Nu^* correlation for planar ducts; for more complex situations, these may be obtained from numerical simulation. It is interesting to note that the term α is referred to as a "conductance," whereas F is generally considered to be a "resistance."

Mass Transfer

Species conservation may be expressed in the form

$$\frac{\partial(\rho_i \varepsilon_i m_j)}{\partial t} + \nabla \cdot (\rho_i \varepsilon_i \mathbf{u}_i m_i) = \nabla \cdot (\Gamma_{ij} \varepsilon_i \nabla m_i) + \varepsilon_i j_i''' \quad (13)$$

where m_j is the mass fraction of species j in phase i. There are no interphase mass transfer terms. Mass sources/sinks have the convective form

$$j_i'''=\dot{m}'''m_{j,t} \tag{14}$$

where $m_{i,\ t}$ is the mass fractions of species i at the "transferred substance state" (T state) [10]. The wall values, required for the Nernst equation, may be computed from [11]

$$m_w=\frac{m_b+m_tB}{1+B} \tag{15}$$

where the mass transfer driving force, B, is obtained approximately as

$$B=\exp(b)-1 \tag{16}$$

and $b=\dot{m}''/g^*$ is a blowing parameter. Mass factions, m_j, may easily be converted to molar fractions, x_j, and vice versa.

The impact of mass transfer on the interphase heat transfer terms above may be incorporated as being approximately given by

$$\frac{h}{h^*}=\frac{b}{\exp(b)-1} \tag{17}$$

where h^* is the heat transfer coefficient for zero mass transfer. Since the magnitude of the contribution of the conduction term in Eq. (12) is rather minor, the term h/h^* in Eq. (17) may reasonably be replaced by α/α^*.

Computational Methodology

Only steady-state cases were considered in this study, and the finite-volume equations may be written [12] for a structured mesh as

$$\begin{aligned} &a_W(\phi_W-\phi_P)+a_E(\phi_E-\phi_P)+a_S(\phi_S-\phi_P)+a_N(\phi_N-\phi_P)\\ &\quad+a_L(\phi_L-\phi_P)+a_H(\phi_H-\phi_P)+S=0 \end{aligned} \tag{18}$$

where W, E, S, N, L, H refer to the west, east, south, north, low, and high neighbors of cell P. In the present scheme, the interphase terms (iii) in Eq. (3) were coded in the form of linearized source terms (v) using the MUSES scheme, described further below, according to

$$S=C(V-\phi_P) \tag{19}$$

where C is a source-term coefficient and V is a source-term value. Since the finite-volume equations are integrated, no distinction need be made between volumetric

and area sources, viz.,

$$S = \int \dot{S}\, dt = \iint_V \dot{S}'''\, dV\, dt = \iint_A \dot{S}''\, dA\, dt \tag{20}$$

Multiply shared space method. The MUSES method was originally developed in the context of heat exchanger networks, and subsequently adapted to simultaneously model both shell- and tube-side transport phenomena, and later still, solid stresses in heat exchangers. It has also been applied to analysis of blast furnaces. Figure 3 illustrates the fundamental mechanism of the MUSES technique as applied to the present problem: A separate space is created for each of the four component materials. For the air and fuel zones, both stack and manifolds were tessellated using a structured mesh, as illustrated. For the single-cell model, no manifolds are required. All redundant regions in the solids and manifolds are blocked. "Halo" or "ghost" cells are used to isolate the three interconnecting regions, as shown in the figure. Porosities, ε, are set to the values given in Table 1, except in the manifolds, where they are set to unity.

Suppose that in the stack, the fuel, air, electrolyte, and interconnect regions each have N_s cells in the horizontal direction and there are N_m cells in the manifolds. Interphase values, V, for Eq. (19), for, say, the fuel–electrolyte pair are obtained as $V(i,j) = \phi[i \pm (N_s + 1), j]$ for every (x, y) pair, a positive sign being associated with the electrolyte-to-fuel source terms and a negative sign with the fuel-to-electrolyte

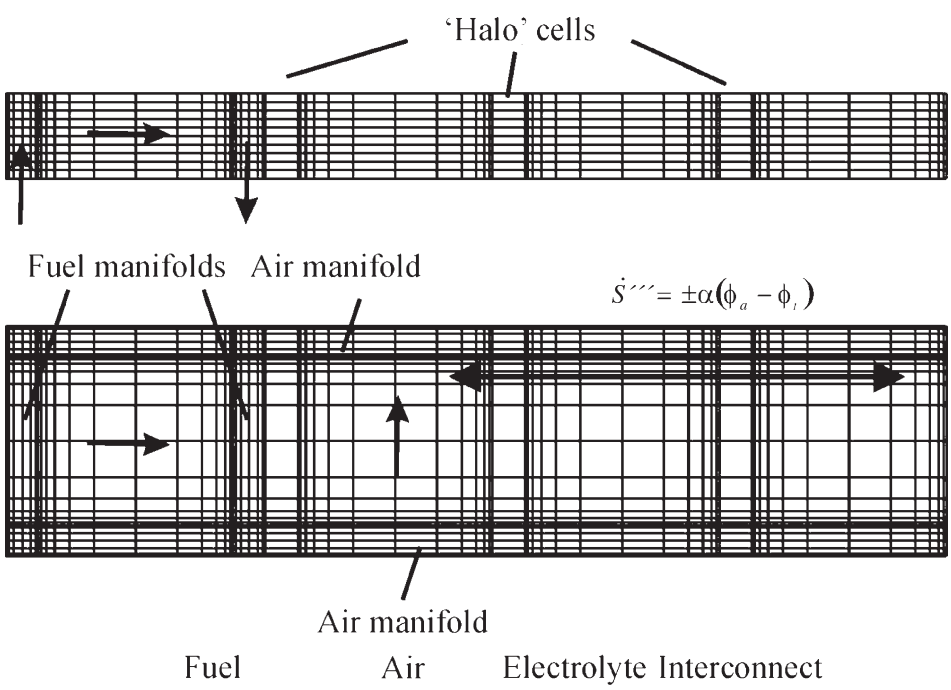

Figure 3. MUSES concept with four "spaces": Fuel, air, electrolyte, interconnect.

sources. Similarly for the air–electrolyte pair, $V(i,j) = \phi[i \pm (2N_s + N_m + 2)]$; the air–interconnect pair; $V(i,j) = \phi[i \pm (3N_s + N_m + 3)]$; and the fuel–interconnect pair, $V(i,j) = \phi[i \pm (2N_s + N_m + 2)]$. This implementation was rendered particularly simple by employing a structured rectilinear mesh. The code used in this project was the general-purpose CFD code PHOENICS [13, 14].

Computational algorithm. Let it be assumed that the following are known: cell voltage, V; inlet flow rates for air and fuel, $\dot{m}_a$; $\dot{m}_f$; and mass fractions of the component species in the air, $m_{O_2,i}$, $m_{N_2,i}$, and in the fuel $m_{H_2,i}$, $m_{H_2O,i}$, respectively. Based on an initial guess field for i'', mass sources/sinks consumed/produced by the reaction, $\dot{m}_{O_2}$, $\dot{m}_{H_2}$, $\dot{m}_{H_2O}$, are deduced from i'' using Faraday's law. The sequence proceeds as follows.

1. Solve the transport equations.
2. Calculate the Nernst potential, Eq. (1), and the local current density, $i'' = (E - V)/r$.
3. Based on the new current density, compute values for r_e, mass sinks/sources, $\dot{m}''_{O_2}$, $\dot{m}''_{H_2}$, $\dot{m}''_{H_2O}$, and heat source, $\dot{q}'''$.
4. Repeat steps 1–3 until convergence is obtained.

Voltage correction. Sometimes it is convenient to prescribe the cell current, and calculate the resulting voltage (galvanostatic condition); at other times it is voltage which is prescribed and current which is obtained (potentiostatic condition). Both situations are encountered. The above methodology is most suitable to the latter. In the galvanostatic situation, which is the *de facto* reality in stack modeling, because of the requirement that overall charge be conserved, we propose adjusting or correcting the voltage iteratively until the desired current is reached. In the approach taken here, the term $\partial V/\partial i'' = -r$ is computed, and the voltage adjusted from $V = V^* + \tilde{V}$, where V^* is the prescribed value of V at the previous iteration and $\tilde{V}$ is a voltage correction:

$$\tilde{V} = -r\left(\bar{i}'' - \bar{i}''^*\right) \tag{21}$$

where $\bar{i}''$ is the desired value of the current density, $\bar{i}''^*$ is the present value of current density obtained by summation from local values, and r is an estimate of the average resistance, which need not be exact.

Detailed Numerical Model

A previously developed detailed numerical model [4] was used for comparison with the model devised above. Rate equations were not assumed in the DNM; the diffusion terms $\Gamma \operatorname{grad} \phi$ were solved directly with a fine mesh concentrated at fluid–wall regions, as appropriate. The material and transport properties were prescribed for each region corresponding to fuel, air, electrolyte, and interconnect. Volume averaging was not therefore required.

RESULTS AND DISCUSSION

Figures 4 and 5 are a comparison of the distributed resistance analogy (DRA) and the detailed numerical method (DNM) for a single cell, with no manifolds, under potentiostatic conditions with cell voltage $V = 0.75$ V. Figures 4*a* and 4*b* show contours of current density, Figures 4*c* and 4*d* show Nernst potential, Figures 4*e* and 4*f* are temperature plots. Figures 5*a*–5*d* show mass fraction of H_2 and H_2O near the anode in the fuel, Figures 5*e* and 5*f* are corresponding cathodic O_2 mass fractions in the air.

The H_2 contours are nominally perpendicular to, and decreasing along, the fuel streamlines. A similar profile is observed for the H_2O contours, though these increase in magnitude due to the production of water by the electrochemical reaction. The O_2 profile is seen to be nominally decreasing in a direction perpendicular to the flow field. Because the current density is presumed identical at the anode and cathode (for a sufficiently thin electrolyte), the source terms of H_2, H_2O, and O_2 are coupled, and the mass fraction contours are skewed somewhat, this effect being more pronounced at high current densities. The Nernst potential appears to be most influenced by the H_2 and H_2O mass fractions, since the sum of these terms in Eq. (1) is larger in magnitude than that of the O_2 term, due to the stoichiometry of the reaction. However, E decreases as the concentrations of O_2 and H_2 are reduced and that of the H_2O increases, going from inlet to outlet, as would be expected. Both cell temperature and Nernst potential affect the current density: The temperature contours, Figures 4*e* and 4*f*, show a maximum toward the air outlet; if the power dissipated in the electrolyte were entirely uniform (constant current density and electrolyte resistance), the maximum would be at the top right corner, corresponding to the common air–fuel outlet for cross-flow. The highly conducting metallic interconnect serves as a thermal fin [6], smoothing out temperature gradients in the horizontal plane; if it were not present, the difference in temperature between inlet and outlet would be much greater (a highly undesirable situation from the perspective of mechanical design). The electrolyte resistance is inversely proportional to the temperature, thus the current density increases in high-temperature regions, since $i'' = (E - V)/r$. Similarly, large values of the local Nernst potential will also tend to increase the local current density. Thus it is seen that there is a complex interaction between physical chemistry and transport phenomena; the subject referred to as physical–chemical hydrodynamics [15].

It can be seen that there is excellent agreement between the results of the DNM, obtained by direct solution of the finite-volume equations, corresponding to the principles of balance of mass, momentum, energy, and species, and the DRA, which is based on the substitution of drag, heat, and mass transfer coefficients (i.e., rate equations) in place of the diffusion (viscous, conduction) terms in the conservation equations. This indicates that the substitution of appropriate values for the interphase heat transfer coefficients and distributed resistance coefficients leads to very reasonable results at a fraction of the cost, in terms of computer time and memory. It is particularly encouraging to note that the 1-D mass transfer analysis, Eqs. (15) and (16), yields wall mass fractions of H_2, H_2O, and O_2 in close agreement with the detailed calculations, since there are significant variations between m_w and m_b.

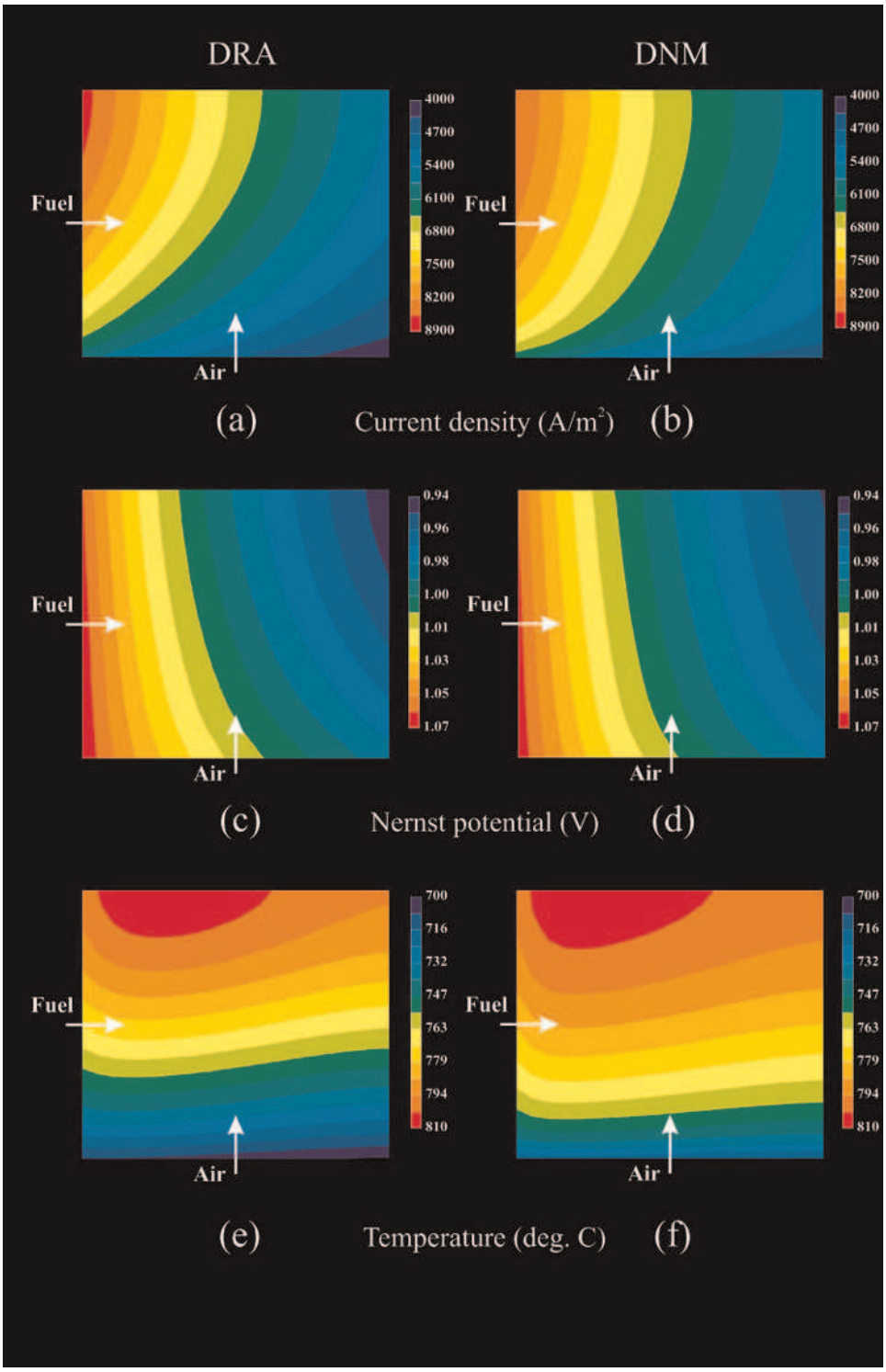

Figure 4. Single cell, plan view, potentiostatic condition, $V = 0.75$ V.

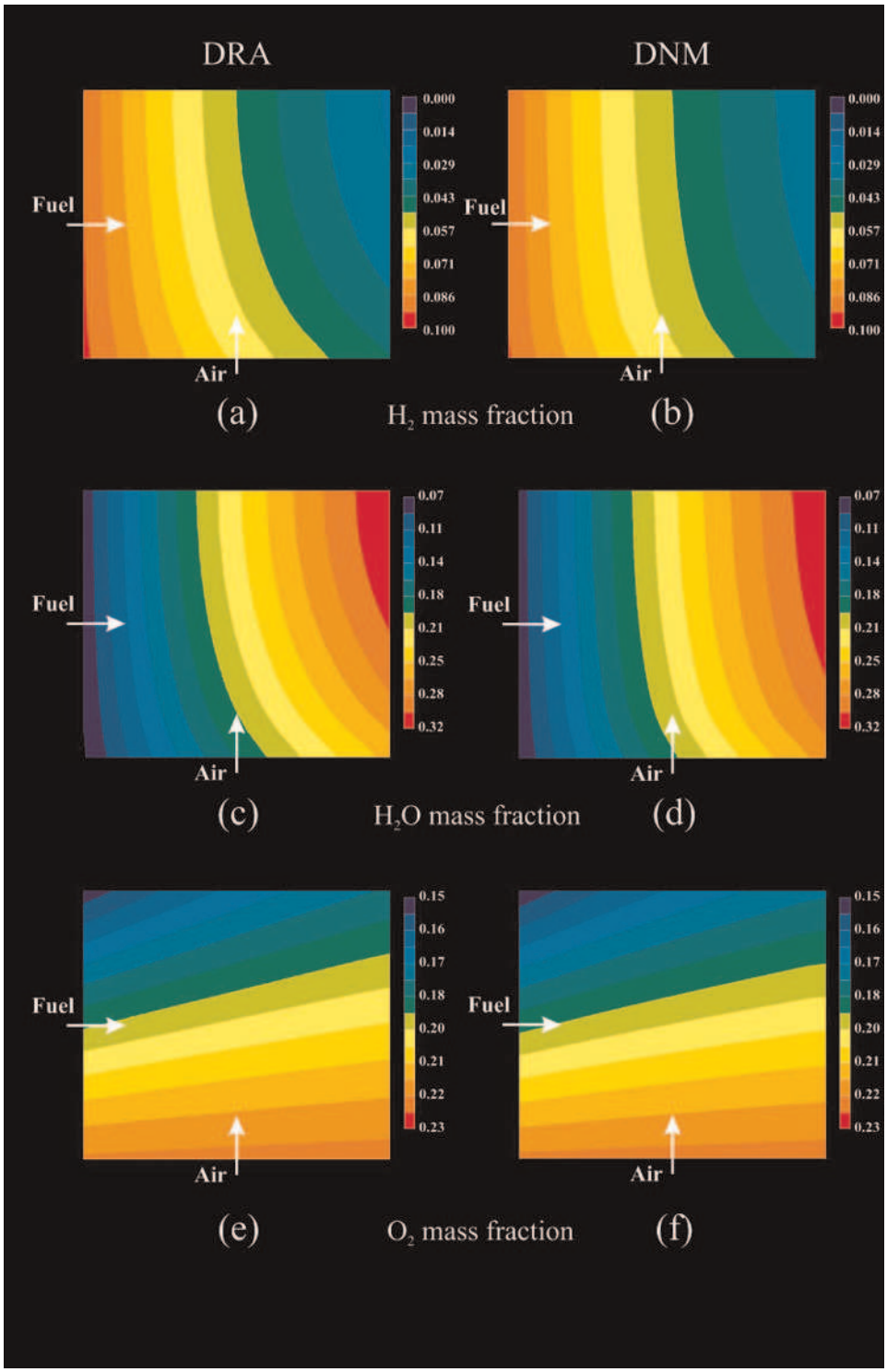

Figure 5. Single cell, plan view, potentiostatic condition, $V = 0.75$ V.

Figure 6 shows calculations for a 10-cell manifold stack assembly, obtained for a galvanostatic condition with a mean current density of $\vec{i}'' = 4{,}000\ \mathrm{A/m^2}$. Figures 6*a* and 6*b* show elevation views of velocity vectors for the air-side flow field at the center of the stack based on calculations obtained using the DRA and the DNM methods. Figures 6*c* and 6*d* show the associated pressure distributions, Figures 6*e* and 6*f* are mass fraction of O_2. Figures 6*g* and 6*h* show the temperature distributions obtained for the air space (DRA) and the entire stack (DNM). Figures 6*i* and 6*j* show the current density and Nernst potential obtained using the DRA.

Inspection of Figures 6*a*–6*h* reveals that even though the fine detail of the motion is lost, realistic pressure and velocity data are obtained. Figure 6*b* shows the characteristic parabolic-shaped velocity profile associated with fluid flow in planar ducts. This profile is clearly absent from the DRA vector field of Figure 6*a*, however, the pressure fields are in close agreement. The results illustrate that the manifold–stack assembly is well designed hydraulically, as pressure and velocity fields are uniform throughout stack assembly. The article by Beale et al. [5] contained an analysis of a stack in which the pressure and velocity distributions were nonuniform. The latter situation arises when pressure gradients in the manifolds are not small in comparison to those in the fuel cell passages. This can be a problem in large stacks, in which suction/injection of fluid from the inlet/outlet manifolds into the stack results in the pressure gradient decreasing/increasing away from the inlet/exits at the manifolds. Inertial effects alone will cause the pressure gradient across the stack at the top to be less than across the bottom, resulting in variations in the flow field. This tendency can be minimized by ensuring that the cell passages are small in comparison to the manifolds. Berman [16] presented an analysis appropriate to viscous flow in planar channels with injection/suction at both boundaries; similar solutions for mass transfer at only one boundary were presented in [17, 18].

The O_2 mass fractions are reasonably constant from cell to cell in the vertical direction, with good agreement between the two methodologies. The reader will note that values of m_{O_2} plotted in Figure 6*e* are bulk values, unlike those shown in Figure 5*e*; which are wall values. Close inspection of Figure 6*f* reveals significant variation in m_{O_2} across individual microchannels: The gradients increase with increasing current density; the maximum current occurs for a short circuit, at which point $V \to 0$, and the so-called diffusion limit is reached, whereby mass transfer, not electrical resistance or charge transfer, is the rate-limiting factor. At high current densities it is important that Eqs. (15) and (16) be invoked to avoid overprediction of the Nernst potential, which would occur if bulk values were used.

Figures 6*g* and 6*h* show temperature distribution assuming adiabatic (well-insulated) thermal boundary conditions. The overall agreement between the DRA and the DNM is good. Plan views of the temperature distribution are qualitatively similar to those obtained for the single-cell geometry, Figures 4*e* and 4*f*. The DNM results exhibit a characteristic "zigzag" pattern, which has been noted in other studies, e.g., of heat exchangers [19, 20]. This is due to the fact that the fuel, air, electrolyte, and interconnect are all at slightly different temperatures. The electrolyte is always at a slightly higher temperature than both the air and fuel passages, due to Joule heating. Heat transfer from the electrode–electrolyte assembly to the bulk of the fluids is a function not only of the temperature difference and the heat transfer

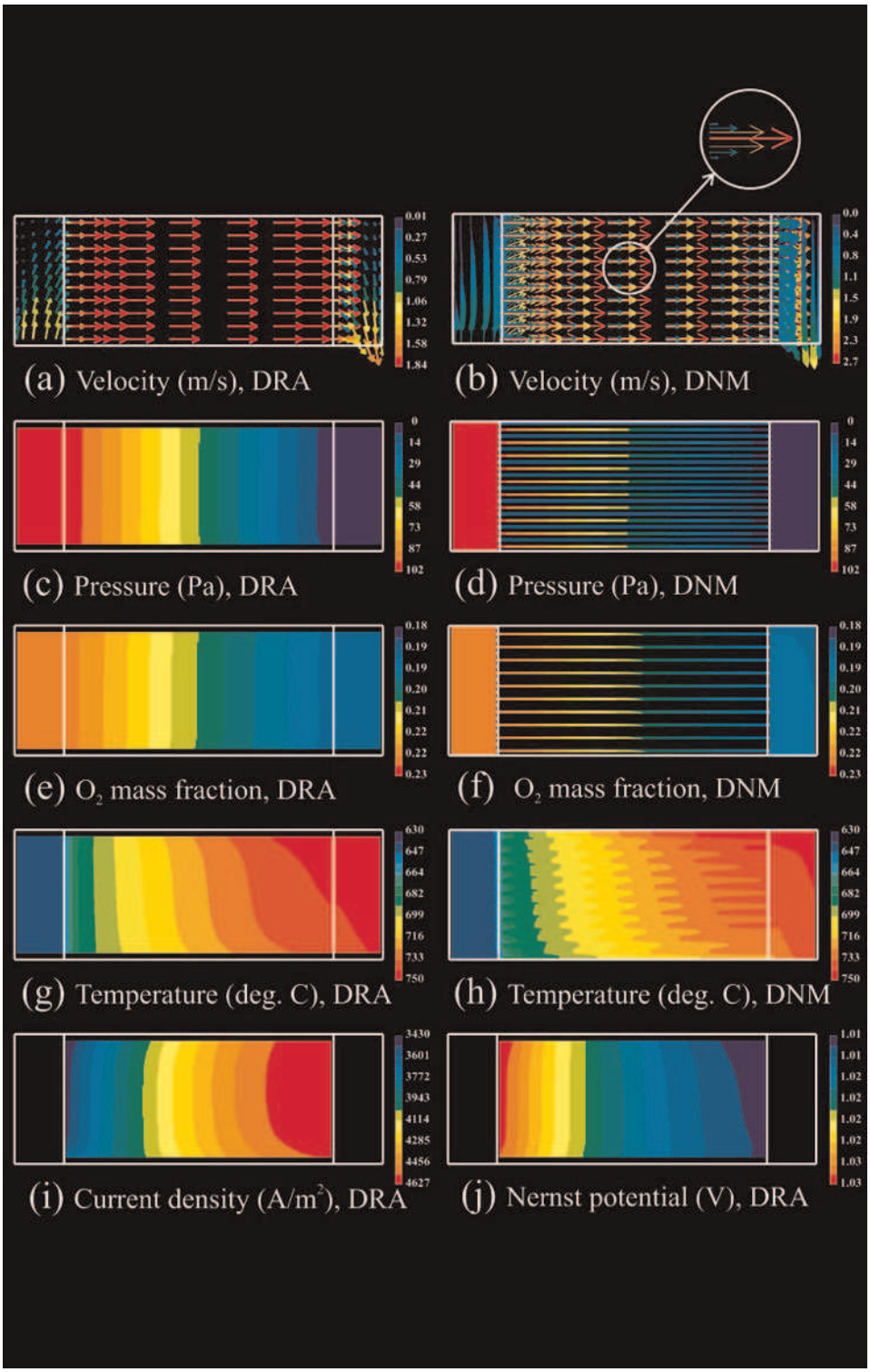

Figure 6. Ten-cell stack, elevation view, galvanostatic condition, $\bar{i}'' = 4,000\ \mathrm{A/m^2}$.

coefficients, $\alpha_{fe,}$ $\alpha_{ae,}$, etc., but also of the thermal capacitances of the fluids, $\dot{c} = \dot{m}c_p$. In general, the air and fuel passages will not be at precisely the same temperature. Because of the "ordering of the streams" in the vertical direction in the stack assembly, there are secondary temperature gradients in the vertical direction. These are readily apparent in Figure 6*h*. In a previous study [6], it was shown that these occur even when the heat source term, $\dot{q}'''$, is uniform.

For single fuel cells it is quite possible to perform detailed CFD calculations using the DNM; and indeed a number of code vendors are now offering fuel cell models to their clients as a software product. For large-scale industrial stacks, such methods cannot readily be applied at the present time, since the computing requirements far exceed what is generally available to the fuel cell manufacturer. The reader will appreciate that for the most part, fuel cells are fabricated with rectangular (rather than planar) passages, and that there will be hundreds or even thousands of these microchannels: It is necessary to mesh each microchannel with a fine-scale mesh, in order to capture the diffusion terms near the air/fuel walls. This is simply not tenable at the present time using normal-sized computers. Moreover, at high current densities, when there is strong suction of oxygen from air, great care is required to concentrate the mesh. The DRA demonstrates that it is not necessary to use a detailed CFD code to obtain reliable performance calculations for SOFCs and stacks.

Convergence and Numerical Considerations

Convergence was achieved, by and large, without difficulty. Spalding [21, 22] notes that the two-fluid DRA methodology is similar to an Eulerian two-phase flow formulation; in the event that interphase transfer dominates all other terms in the finite-volume equations, stability may be a matter for concern in the absence of a partial elimination algorithm or equivalent. Some oscillations were observed in the residual plots, though these did converge without difficulty when relaxation was used. Coding the interphase transfer terms as source terms is a compromise: A fully coupled solver would speed up the convergence times, compared to the segregated scheme employed here; however, the MUSES method allowed a physical model to be developed in a timely manner without rewriting the CFD source code.

The voltage-correction algorithm converged without difficulty for the galvanostatic case, provided a reasonable initial guess was made for the cell voltage. The reader will note that if the $V - i''$ curve is linear, and the choice of r in Eq. (21) is correct, then the correct cell value will be predicted after only one iteration. In practice, though, the $V - i''$ curve is nonlinear, and since r is only an estimate of the mean cell resistance, some iteration is required. An advantage of the voltage-correction approach adopted here is that r need not be exact, and by increasing/decreasing this "resistance," over/underrelaxation may readily be facilitated. It is of course fully acceptable to compute the average resistance by integration, and obtain the voltage as a function of both this and the prescribed mean current density by numerical integration. The same result will ultimately be achieved.

The reader will note that the original form of the DRA [1] required it to be modified for the stack model, since otherwise secondary thermal effects would be lost, due to local volume averaging. Recall that the interphase heat transfer terms

were computed as pairs of values, e. g., $\dot{q}'''_{ae} = -\dot{q}'''_{ea} = \alpha_{ae}[T_a(k) - T_e(k)]$ for the air–electrolyte pair, where $k = 1, 2, 3, \ldots, n_z$. A similar prescription was made for the air–interconnect and fuel–interconnect pairs. For the fuel-to-electrolyte pair, however, the sources were computed as $\dot{q}'''_{fe} = \alpha_{fe}\left[T_f(k+1) - T_e(k)\right],\ k = 2,\ 3,\ 4, \ldots,\ n_z$ and $\dot{q}'''_{ef} = \alpha_{fe}\left[T_e(k-1) - T_f(k)\right],\ k = 1,\ 2,\ 3, \ldots,\ n_z - 1$. Since the computational cells in the z direction coincided with the fuel cells, $n_z = 10$; this simple modification resulted in the secondary temperature effect being recovered, as shown in Figure 6*g*. A minor disadvantage of this technique in the present form is that the computational cells must therefore coincide with the actual fuel cells in the vertical direction for the methodology to succeed.

CONCLUSIONS AND FUTURE WORK

The DRA has been shown to be an effective method for prediction of transfer phenomena in solid oxide fuel cells. In addition to fluid flow, heat and mass transfer, detailed electrochemical calculations have now been performed for the first time using the DRA. The results were validated using a DNM. The main advantage of the DRA is that it allows reliable calculations to be obtained for nonuniform flow and current density fields, at a fraction of the computational cost needed to perform detailed CFD calculations. The original DRA method, as applied to heat exchanger design, was modified substantially to account for concentration gradients near wall regions. This is required because the Nernst equation, Eq. (1), is based on wall values, not bulk values. The success of the DRA methodology is critically dependent on the numerical values of the distributed resistances, F, and overall heat transfer coefficients, α. The latter were corrected for mass transfer effects as outlined in the article; the former were not, as it was ascertained that the driving force for momentum transfer is one order of magnitude smaller than that for heat/mass transfer. Of course, the rate of heat transfer occurs at neither constant temperature nor constant heat flux, so the choice of α is to be considered an idealization of reality. The ability to disable the diffusion terms in some, but not all, directions allowed for heat conduction in the stainless steel interconnects in the horizontal plane to be correctly incorporated into the model.

It is maintained that the subgrid models developed for this research program are sufficiently detailed to characterize SOFCs for engineering purposes. However, there is substantial scope for further model development and improvement: Chemical kinetics will be accounted for using a Butler-Volmer equation, in place of the simple lumped resistance formulation above. The electrochemical heating effect (at the anode) needs to be separated from the Joule term within the bulk of the electrolyte. Murthy and Federov [23] have suggested that neglect of thermal radiation in SOFCs can lead to substantial overprediction of the temperature field, and it is the authors' intention to investigate these claims in the future. Some CFD codes now calculate the electric field potential in the electrolyte and metallic interconnects, in place of the one-dimensional Nernst equation. For thin electrolytes a Nernst formulation is considered perfectly adequate; however, there would be no problem in solving the electric potential using the distributed resistance analogy, and this would be a natural extension to the work described in this article. Treatment of the electric potential

is essentially the same as that for temperature in the solid (interconnect and electrolyte) spaces, i.e., a set of coupled diffusion–source equations.

In most practical planar SOFCs, the fluid channels are of rectangular rather than planar geometry, with ribbed interconnects, essentially low-aspect-ratio rectangular fins. It is straightforward to compute conduction shape factors for heat transfer and electrical resistance calculations. Electrodes of finite thickness are typically in the form of porous media with an associated bulk-to-interface mass transfer driving force. In addition, there usually are nonparticipating porous gas diffusion layers (GDLs) to assist transport of the fuel and air to the electrodes from the microchannels. Some additional research is needed to characterize mass transfer within the gas diffusion layers and electrolytes. Following such an analysis, the DRA may readily be applied to more complex geometries, either by increasing the number of spaces in the MUSES technique to include these additional layers (GDLs, electrodes, etc.), and/or by correlating mass transfer in the porous media terms as a function of geometry and blowing parameter.

Although the SOFC geometry considered in this study had a simple form, and flow fields were relatively uniform, there are many other types of fuel cell in which the flow fields are far from uniform. For example, cylindrical SOFCs exist which offer certain advantages from the perspective of mechanical design. In the automobile industry, proton-exchange membrane fuel cells (PEMFCs) are considered as a potential replacement for the internal combustion engine. PEMFCs are frequently designed with the flow passages in the form of serpentine-shaped channels. For such situations the DRA would prove of great utility, not only for stack-level models, but also for analysis of single cells.

REFERENCES

1. S. V. Patankar and D. B. Spalding, A Calculation Procedure for the Transient and Steady-State Behaviour of Shell-and-Tube Heat Exchangers, Imperial College Mechanical Engineering Rep. EF/TN/A/48, Imperial College of Science and Technology, London, UK, 1972.
2. S. B. Beale and D. B. Spalding, Numerical Study of Fluid Flow and Heat Transfer in Tube Banks with Stream-wise Periodic Boundary Conditions, *Trans. Can. Soc. Mech. Eng.*, vol. 22, pp. 394–416, 1998.
3. A. J. Bard and L. R. Faulkner, *Electrochemical Methods*, Wiley, New York, 2001.
4. W. Dong, S. B. Beale, and R. J. Boersma, Computational Modelling of Solid Oxide Fuel Cells, *Proc. 9th Conf. CFD Soc. Canada—CFD 2001*, Waterloo, Canada, pp. 382–387, 2001.
5. S. B. Beale, A. Ginolin, R. Jerome, M. Perry, and D. Ghosh, Towards a Virtual Reality Prototype for Fuel Cells, *PHOENICS J. CFD*, vol. 13, pp. 287–295, 2000.
6. S. B. Beale, S. V. Zhubrin, and W. Dong, Numerical Studies of Solid-Oxide Fuel Cells, *Proc. 12th Int. Heat Transfer Conf.*, Grenoble, France, pp. 865–870, 2002.
7. S. B. Beale, Y. Lin, S. V. Zhubrin, and W. Dong, Computer Methods for Performance Prediction in Fuel Cells, *J. Power Sources*, vol. 11, pp. 79–85, 2003.
8. M. Jacob, *Heat Transfer*, Wiley, New York, 1949.
9. R. K. Shah and A. L. London, Laminar Flow Forced Convection in Ducts, in T. F. Irvine and J. P. Hartnett (eds.), *Advances in Heat Transfer*, supp. 1, Academic, New York, 1978.
10. D. B. Spalding, A Standard Formulation of the Steady Convective Mass Transfer Problem, *Int. J. Heat Mass Transfer*, vol. 1, pp. 192–207, 1960.

11. S. B. Beale, Calculation Method for Mass Transfer in Fuel Cells, *J. Power Sources*, vol. 128, pp. 185–192, 2004.
12. S. V. Patankar, Numerical Heat Transfer and Fluid Flow, Hemisphere, New York, 1980.
13. D. B. Spalding, Four Lectures on the PHOENICS Code, Computational Fluid Dynamics Unit Rep. CFD/82/5, Imperial College of Science and Technology, London, UK, 1982.
14. D. B. Spalding, PHOENICS 1984. A Multi-dimensional Multi-phase General-Purpose Computer Simulator for Fluid Flow, Heat Transfer and Combustion, Computational Fluid Dynamics Unit Rep. CFD/84/18, Imperial College of Science and Technology, London, UK, 1984.
15. V. G. Levich, *Physicochemical Hydrodynamics*, Prentice Hall, Englewood Cliffs, NJ, 1962.
16. A. S. Berman, Laminar Flow in Channels with Porous Walls, *J. Appl. Phys.*, vol. 24, pp. 1232–1235, 1953.
17. J. Jorne, Mass Transfer in Laminar Flow Channel with Porous Wall, *J. Electrochem. Soc.*, vol. 129, pp. 1727–1733, 1982.
18. P. Lessner and J. S. Newman, Hydrodynamics and Mass-Transfer in a Porous-Wall Channel, *J. Electrochem. Soc.*, vol. 131, pp. 1828–1831, 1984.
19. P. J. Coelho, Mathematical Modeling of the Convection Chamber of a Utility Boiler—An Application, *Numer. Heat Transfer A*, vol. 36, pp. 411–428, 1999.
20. P. J. Coelho, Mathematical Modeling of the Convection Chamber of a Utility Boiler—The Theory, *Numer. Heat Transfer A*, vol. 36, pp. 429–447, 1999.
21. D. B. Spalding, Methods of Calculating Heat Transfer within the Passages of Heat Exchangers, Computational Fluid Dynamics Unit Rep. HTS/81/4, Imperial College of Science and Technology, London, UK, 1981.
22. D. B. Spalding, The Calculation of Heat-Exchanger Performance, Computational Fluid Dynamics Unit Rep. HTS/81/5, Imperial College of Science and Technology, London, UK, 1981.
23. S. Murthy and A. G. Federov, Radiation Heat Transfer Analysis of the Monolith Type Solid Oxide Fuel Cell, *J. Power Sources*, vol. 124, pp. 453–458, 2003.